CCAT Optics

S. Padin,[a] M. Hollister,[a] S. Radford,[a] J. Sayers,[a] D. Woody,[a] J. Zmuidzinas,[a]
G. Cortes-Medellin,[b] T. Sebring,[b] G. Stacey[b]

[a] California Institute of Technology, Pasadena CA 91125;
[b] Cornell University, Center for Radiophysics and Space Research, Ithaca NY 14853

CCAT Optics

S. Padin*[a], M. Hollister[a], S. Radford[a], J. Sayers[a], D.Woody[a], J. Zmuidzinas[a],
G. Cortes-Medellin[b], T. Sebring[b], G. Stacey[b]

[a]California Institute of Technology, Pasadena CA 91125;
[b]Cornell University, Center for Radiophysics and Space Research, Ithaca NY 14853

ABSTRACT

CCAT will be a 25 m diameter, submillimeter-wave telescope. It will be located on Cerro Chajnantor in the Atacama Desert, near ALMA. CCAT will be an on-axis, Ritchey-Chrétien design with an active primary to compensate gravitational deformations. The primary mirror will have 162 segments, each with $\sim 0.5 \times 0.5$ m reflecting tiles on a $\sim 2 \times 2$ m, insulated, carbon-fiber-reinforced-plastic subframe. CCAT will be equipped with wide-field, multi-color cameras and multi-object spectrometers at its Nasmyth foci. These instruments will cover all the atmospheric windows in the $\lambda = 0.2$ to 2 mm range. The field of view at the Nasmyth foci will be 1°, so CCAT will be able to support cameras with a few $\times 10^4$ detectors (spaced 2 beamwidths) at $\lambda = 1$ mm to a few $\times 10^6$ detectors (spaced half a beamwidth) at $\lambda = 350$ μm. Single instruments of this size are probably impractical, so we will break the field into smaller pieces, with a separate sub-field camera for each piece. The cameras will require some relay optics to couple the fairly slow beam from the telescope to the detectors. A reflective relay for 1° field of view is too large to be practical, so we plan to use a compact, cold, refractive relay in each sub-field camera.

Keywords: Radio astronomy, submillimeter telescopes

1. INTRODUCTION

CCAT will be a 25 m diameter, Ritchey Chrétien (RC) telescope, operating in the 0.2 to 2 mm wavelength range. It will be located at an altitude of 5600 m on Cerro Chajnantor in Northern Chile, near ALMA. This is one of the best submillimeter sites on Earth.[1,2] It is also easily accessible. Proximity to ALMA will maximize the opportunity for high-resolution follow up of new sources found in CCAT surveys.

CCAT will be equipped with wide-field, multi-color cameras for surveys, and multi-object spectrometers for spectroscopic follow up. It will observe structures on all scales ranging from Kuiper Belt objects to clusters of galaxies, but its immediate impact is likely to be in tracing the process of galaxy formation from the first giant starbursts. CCAT will be sensitive. A small, first-light, $\lambda = 350$ μm camera might have 128×128 absorber-coupled detectors spaced $0.5\mathcal{F}\lambda$, where $\mathcal{F}$ is the focal ratio at the detectors, giving a field of view (FoV) of 3.7'. With this camera, CCAT will map 1 deg^2 to the confusion limit at 5σ in ~ 400 hr (see Table 1). The 1 deg^2 image will contain tens of thousands of submillimeter galaxies at redshift ~ 2, and a few strongly lensed galaxies at redshift > 6.[3,4] Photometry in a few bands will yield rough estimates of the redshifts of these objects, but a multi-object spectrometer (MOS) will clearly be needed for follow up. CCAT will eventually be equipped with cameras covering all the atmospheric windows in the $\lambda = 0.2$ to 2 mm range, with a FoV up to 1°, and a MOS that can select tens of objects from the 1° FoV.

Table 1. CCAT continuum mapping speed.

λ	Beamwidth	NEFD	Confusion	Time to confusion	Time to map 1 deg^2
μm	arcsec	mJy	mJy	s	hr
350	3.5	14.4	1.3	3067	448
2000	20	2.3	0.2	3306	483
		1σ in 1 s	30 beams/source	5σ	1st light camera with 3.7' FoV,
			1σ		confusion at 5σ, 50% efficiency

*spadin@caltech.edu; phone 626 395 4079

Table 2. CCAT optical parameters.

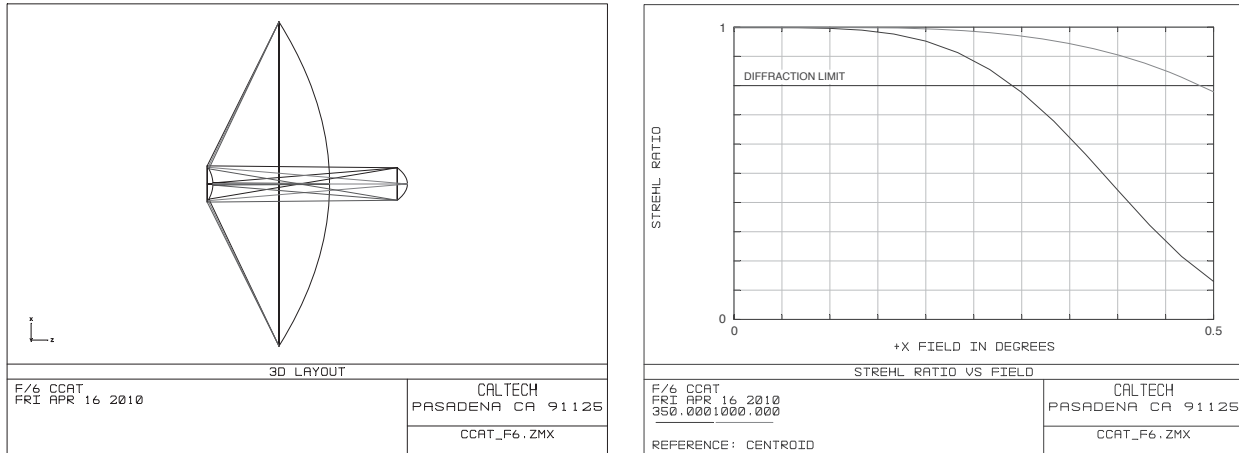| Parameter	Symbol	Value	Units
Primary diameter	D_1	25	m
Primary focal ratio	F_1	0.4	
Final focal ratio	F	6	
Back focal distance	b	6	m
Secondary to tertiary separation	d_2	12	m
Field of view	FoV	1	deg

Figure 1. Optical layout for the basic CCAT design (left) and Strehl ratio vs. field angle (right) at $\lambda = 1$ mm (upper curve) and $\lambda = 350$ μm (lower curve).

This paper gives an overview of the telescope optics and concepts for camera relay optics. The material is broken up into 4 sections. In Section 2 we describe the optical design of the basic telescope. In Section 3 we describe the mirrors and give estimates of wavefront and pointing errors. In Section 4 we present a sub-field camera concept for wide FoV cameras. In Section 5 we describe how some existing instruments might be used on CCAT.

2. TELESCOPE DESIGN

CCAT will be an on-axis design. We chose this because most CCAT observations will be at the shorter submillimeter wavelengths where the transmission of the atmosphere is only $\sim 50\%$. For these observations, there is
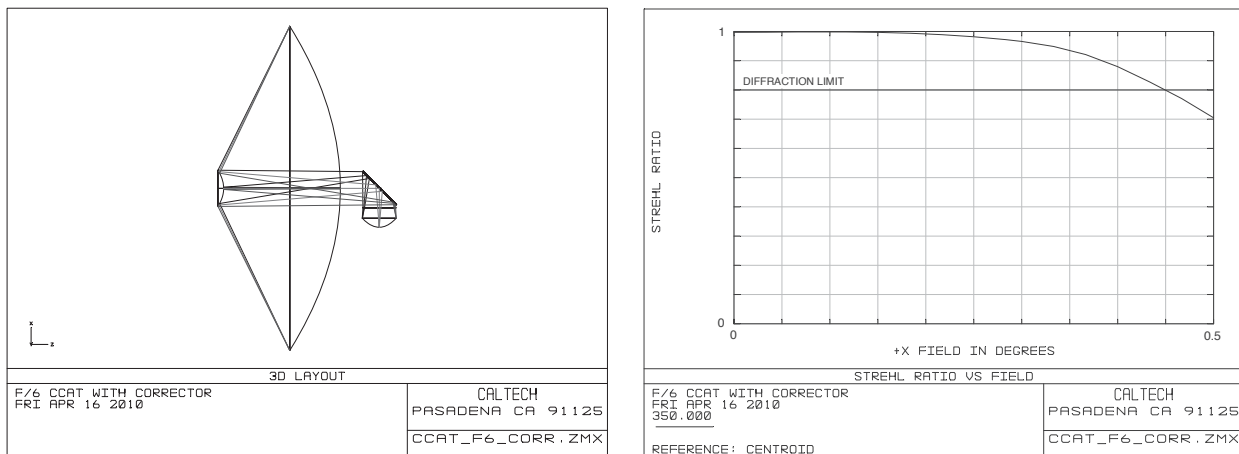

Figure 2. CCAT optical layout with a corrector plate (left) and Strehl ratio vs. field angle (right) at $\lambda = 350$ μm.
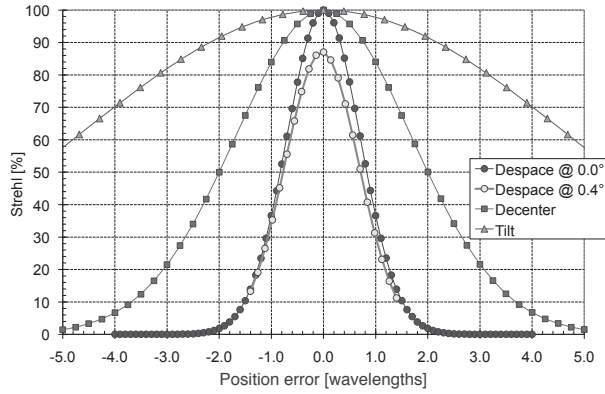
Figure 3. Strehl ratio vs. secondary position error at the field center and Strehl ratio vs. despace at $0.4°$ field angle. Tilt is in wavelengths across the secondary diameter for a rotation about the vertex of the secondary.
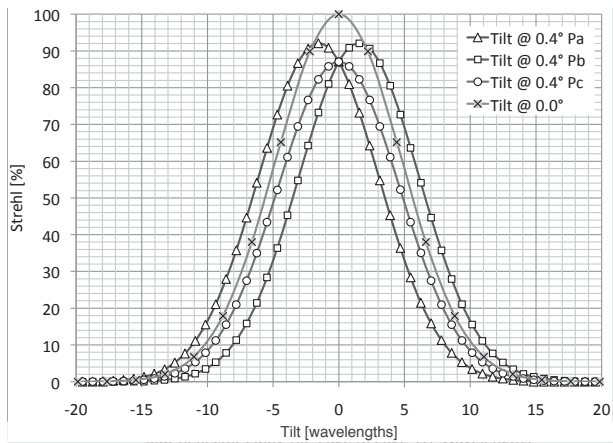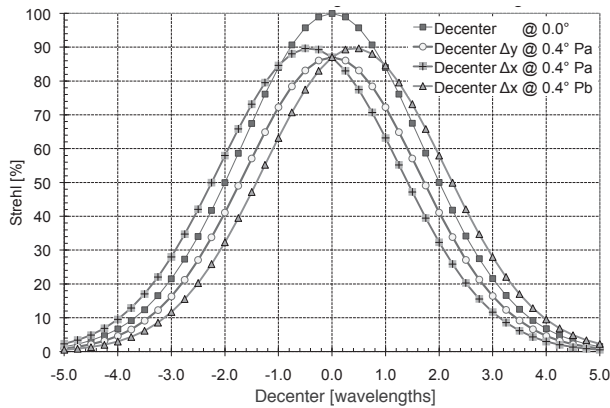

Figure 4. Strehl ratio vs. secondary decenter (left) and tilt (right) at various field angles. Tilt is in wavelengths across the secondary diameter for a rotation about the vertex of the secondary. Pa, Pb and Pc are field offsets of $(-0.4°, \ 0)$, $(0.4°, \ 0)$, and $(0, \ 0.4°)$.
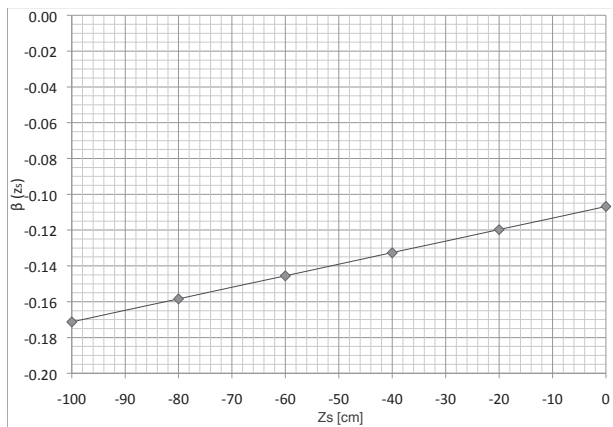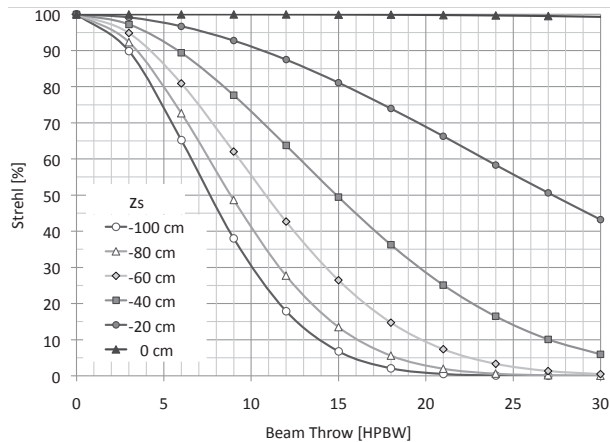
Figure 5. Strehl ratio degradation vs. beam throw due to chopping the secondary (left) and ratio of beam throw to secondary tilt vs. center of rotation (right). HPBW $= 1.22\lambda/D_1$ is the half power beamwidth. Zs is the distance from prime focus to the center of rotation of the secondary. Zs $= 0$ puts the center of rotation at prime focus and Zs $= -100$ cm puts the center of rotation at the vertex of the secondary. β is the ratio of beam throw to secondary tilt. The line in the right plot is the best fit model $\beta = -\left[a/f + b\left(1/f_1 - 1/f\right) \mathrm{Zs}\right]$, with $a = 1.602$ m and $b = 0.6911$.

little to be gained from a more expensive off-axis telescope that eliminates just a few percent scattering from the secondary and its support. At millimeter wavelengths, the loss through the atmosphere is just a few percent, so scattering is more important, especially for observations of low surface brightness emission, e.g., the Sunyaev-Zel'Dovich effect.[5] To support these observations, CCAT will have an absorber-covered secondary support to reduce scan-synchronous variations in scattering. Systematic errors for CCAT will be dominated by 1% scattering from the secondary, 1-2% scattering from the support, and 1-2% scattering from the gaps between the primary mirror segments. Most CCAT instruments will be wide-field, and hence large, so we chose to support just the 2 Nasmyth foci.

CCAT will have a fast primary to minimize the size and cost of the dome. This is an important choice because the cost of the dome is large ($\sim 25\%$ of the cost of the telescope) and it scales at least with surface area. The dome will be a calotte design like that chosen for the Thirty Meter Telescope, but without the complicated venting arrangements that are needed for an optical telescope.[6,7] The distance from the center of a calotte dome to the plane of the hole is $r = \frac{1}{2}\left(D_{\text{dome}}^2 - D_{\text{hole}}^2\right)^{1/2}$, where D_{dome} and D_{hole} are the diameters of the dome and hole respectively. The telescope beam must clear the hole, so $D_{\text{hole}} > D_1$ where D_1 is the diameter of the primary. $D_{\text{hole}} = 1.2 \times D_1$ gives enough clearance for small spillover on the dome. The secondary must also be inside the dome to reduce the effects of wind buffeting, so the secondary to elevation axis separation (i.e., the secondary to tertiary separation) must be $d_2 < r$. The primary vertex must be $\sim D_1/10$ above the elevation axis to provide enough space for the support structure behind the center of the primary. Thus, $d_2 \approx f_1 + D_1/10$, where f_1 is the focal length of the primary. The primary focal ratio is then $F_1 = f_1/D_1 < \frac{1}{2}\left(D_{\text{dome}}^2/D_1^2 - 1.2^2\right)^{1/2} - 0.1$. For CCAT, $D_1 = 25$ m, so $D_{\text{dome}} = 35$ m requires $F_1 < 0.26$. This is too fast for good image quality with reasonable alignment tolerances. $D_{\text{dome}} = 40$ m requires a more reasonable $F_1 < 0.43$. CCAT will have $D_{\text{dome}} = 40$ m, $F_1 = 0.4$, and $d_2 = 12$ m (see Table 2).

CCAT will spend a substantial fraction of its observing time on surveys, finding sources that can be followed up with spectrometers on CCAT and at high resolution with ALMA. Survey speed is an important consideration, especially for finding rare objects such as the highest redshift galaxies, so we chose a wide-field RC optical configuration (see Fig. 1). The disadvantage of the RC design is that we cannot change the secondary to give a different final focal length. This is not a serious limitation because most CCAT instruments will require some relay optics to couple the detectors to the telescope. CCAT's FoV will be limited only by the optical design of the telescope, not by the mechanical structure. This means we will be able take full advantage of the available FoV as larger cameras become possible. The basic RC telescope design has $\sim 1°$ FoV at millimeter wavelengths (see Fig. 1). The FoV is limited by curvature of the focal surface, so $1°$ is a fairly hard limit. At submillimeter wavelengths, aberrations limit the FoV to $\sim 0.5°$. In this case, the FoV can be increased by adding a corrector. A reflective corrector is difficult because it requires very large mirrors, but a refractive corrector plate just before Nasmyth focus seems viable. Fig. 2 shows the optical configuration and image quality. With the corrector, CCAT can achieve $\sim 1°$ FoV at the shorter submillimeter wavelengths.

To minimize scattering, we chose the final focal ratio of the telescope to pass the $1°$ FoV to Nasmyth focus through a hole in the primary that is smaller than the secondary. The size of the secondary is $D_2 = D_1 L/f + \text{FoV} \times f_1$, where L is the secondary to image separation, and f is the final focal length.[8] The diameter of the image is $D_I = \text{FoV} \times f$. <1% scattering from the secondary is a reasonable goal, so $D_2 < D_1/10$. For no scattering from the hole in the primary, $D_I < D_2$. The final focal ratio is then $F = f/D_1 < 1/\left(10 \times \text{FoV}\right)$. For $1°$ FoV, $F < 5.7$. CCAT's FoV is actually slightly smaller than $1°$, so we chose $F = 6$. A smaller secondary gives lower scattering, but it moves the Nasmyth focus closer to the center of the primary. The back focal distance is $b = L - d_1$, where $d_1 \approx f_1\left(1 - D_2/D_1\right)$ is the primary to secondary separation. With $F = 6$, $D_2/D_1 = 0.1$, and $F_1 = 0.4$, $L = 15$ m and $b = 6$ m. Since the secondary to tertiary separation is $d_2 = 12$ m, the Nasmyth focus is just 3 m from the tertiary. This is already closer than we would like, so a smaller secondary is impractical. Table 2 summarizes the key optical design parameters for CCAT. All other optical parameters can be derived from those in the table.

At $\lambda = 1$ mm, a $1°$ FoV camera requires 5×10^4 antenna-coupled detectors spaced $2\mathcal{F}\lambda$. This camera is about the size of the Submillimetre Common-User Bolometer Array 2 (SCUBA-2),[9] so it should be possible to fill CCAT's FoV at $\lambda = 1$ mm at first light, or soon after. At submillimeter wavelengths, the loss in printed antenna structures is high, so we must use absorber-coupled detectors. In this case, maximum mapping speed

is achieved with a detector spacing of $0.5\mathcal{F}\lambda$.[10] The small detectors and small telescope beam make for a very large camera. At $\lambda = 350$ μm, a 1° FoV camera requires 6×10^6 detectors. This is impractical today, but should be possible during CCAT's lifetime.

The plate scale at Nasmyth focus is 2.6 m/deg, so it is impractical to cool a Nasmyth corrector plate for 1° FoV. The corrector must therefore operate at room temperature, so it must be thin and made of low loss material, e.g., Ge or high-resistivity Si. In this case, thin is possible because the corrector has no power. A 1 cm thick Si plate has just a few percent loss at $\lambda = 350$ μm[11] cf. $\sim 50\%$ loss through atmosphere. High resistivity Si is currently available up to 200 mm diameter,[12] so the corrector must be segmented. This is not straightforward because the corrector is not at a focus or a pupil, so gaps or support structures between segments reduce the FoV. We will not need the corrector for millimeter-wave or narrow-field, submillimeter observations, and wide-field, submillimeter cameras are perhaps 10 years away, so we have some time to work on fabrication and anti-reflection (AR) coating techniques. The AR coating should be fairly straightforward because the corrector will be at room temperature. This will give us the option of using multi-layer dielectric coatings[13,14] (e.g., porex, cirlex, or TMM) with thermal expansion coefficients that are not well matched to Si.

The fast primary makes for fairly tight tolerances on the position of the secondary. Figs. 3 and 4 show the Strehl ratio degradation due to secondary decenter, δ, tilt, ε, and despace, z. The Strehl ratio degradation (worst case) is $S_i = \exp - \left[0.05 \left(e_i / c_i \right)^2 \left(350\ \mu\text{m} / \lambda \right)^2 \right]$, where $e = (\delta,\ \varepsilon,\ z)$ and $c = (189\ \mu\text{m},\ 39",\ 78\ \mu\text{m})$. The equivalent rms half wavefront error is $\text{HWFE}_i = k_i e_i$, where $k = (0.0330,\ 0.1597\ \mu\text{m/arcsec},\ 0.0799)$. At $\lambda = 350$ μm, < 1 μm rms HWFE requires $\delta < 30$ μm, $\varepsilon < 6"$, and $z < 13$ μm. These are stringent requirements, particularly for thermal deformations, but they are consistent with the performance of a carbon-fiber-reinforced-plastic (CFRP) secondary support. A 10 m long CFRP secondary support, with coefficient of thermal expansion $\text{CTE} = 2 \times 10^{-7}$ K^{-1}, gives just 2 μm K^{-1} despace error. At the CCAT site, temperature variations during the night are typically 1 K rms,[15] and we can make focus measurements every few hrs, so secondary position errors of just a few μm seem practical. A steel secondary support would give 100 μm K^{-1} despace error. In this case we would need closed-loop control of the secondary position based on, e.g., laser metrology.

For mapping, we will reject atmospheric brightness fluctuations by subtracting low-order components across the detector array, and by scanning the entire telescope at speeds up to 2 deg s^{-1} at millimeter wavelengths and 0.4 deg s^{-1} at submillimeter wavelengths. For spectroscopy, we plan to position switch the entire telescope at a few $\times$0.1 Hz. Faster position switching will require a chopping secondary. We do not plan to implement a chopping secondary at first light, but we will design the secondary support structure to accommodate a chopping secondary in the future. CCAT's fast primary will limit the beam throw for chopping to $\lesssim 6$ beamwidths p-p for $<10\%$ degradation in integration time and chopping about a point near the vertex of the secondary (see Fig. 5). This beam throw will be large enough for observations of compact sources, e.g., submillimeter galaxies.

3. MIRROR DETAILS

The baseline plan for CCAT's primary mirror is a segmented, active surface on a CFRP truss.[16] A 25 m mirror must be active to compensate gravitational deformation, but if the truss has a small enough coefficient of thermal expansion, the surface control can be open-loop, i.e., based on look-up tables for gravity and soak temperature. We do not yet know if a CFRP truss is affordable, so we are also pursuing a design with a steel truss and closed-loop control using segment edge sensors. Both control approaches are technically feasible, and give similar total wavefront errors, as shown in Table 3. The estimates in Table 3 include 1 K rms temperature variations across the structure, 20 K soak temperature change, wind deformations due to 6 ms^{-1} (3rd quartile) outside wind speed (reduced by the dome by a factor 3 at the secondary and a factor 10 at the primary), and deflections due to $0.4°\text{s}^{-2}$ scan acceleration. The structural calculations that support Table 3 are a mix of simple lumped-element models for the mount and secondary support, and finite-element models for the primary truss, segments, and secondary. The estimates are probably good at the 10% level. As expected, the primary is the largest HWFE contribution. The secondary term is only a little smaller because it also includes the effects of secondary position errors. The alignment contribution is for regular (e.g., every 1/2 hr) pointing measurements with a submillimeter science camera, and occasional (e.g., every week) wavefront measurements using a point-diffraction or shearing interferometer.[17,18] The instrument contribution is due to thermal deformation of the instrument mount. The
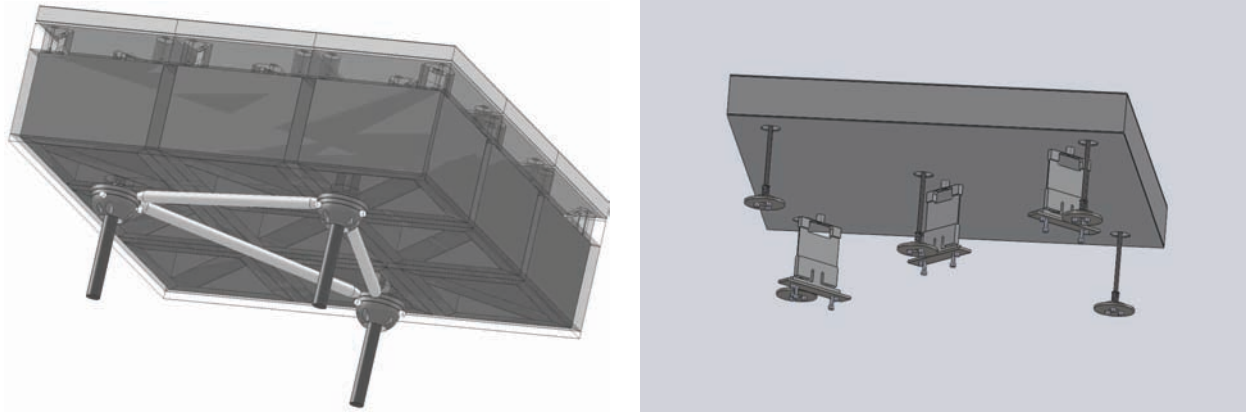
Figure 6. CCAT segment concept (left) and tile detail (right). The long black cylinders on the bottom of the segment are the motorized actuators that attach the segment to the primary truss. The 3 struts between the actuators are the top layer of the truss, but they remain with the segment if it is removed. The transparent material covering the CFRP subframe is insulation. The long thin rods on the back of the tile are the piston adjusters. The plates mounted along the tile diagonal are the lateral position adjusters.

steel truss gives larger pointing errors, partly because it has larger thermal deformations, and partly because it deflects more when the telescope accelerates during scanning. Table 3 also includes HWFE and pointing error estimates for the atmosphere. These estimates are based on 11.2 GHz interferometer measurements at the ALMA site and they include daytime.[19] The higher CCAT site will be a little better. CCAT's HWFE will be limited by the atmosphere $\sim 1/4$ of the time. Pointing will be limited by the atmosphere $\sim 1/2$ of the time. Observations at the shorter submillimeter wavelengths will be therefore be possible $\sim 1/2$ of the time.

The CCAT primary will have $\sim 0.5 \times 0.5$ m machined Al tiles mounted on $\sim 2 \times 2$ m CFRP subframes.[20] The concept is shown in Fig. 6. The tiles will be small enough to give small manufacturing errors and small thermal deformations. The subframes will be large enough to give reasonable control errors if we need a closed-loop control scheme using edge sensors. The subframes will be made of CFRP beams and they will be well insulated, so each subframe will be essentially isothermal. This will reduce the effect of sensor errors due to subframe thermal deformation in a closed-loop control scheme. Each tile will be attached to its subframe with 5 piston adjusters and 3 in-plane adjusters. This over constrained support will allow us to deform the tiles to compensate low-order machining errors. Each subframe will be attached to the truss with 3 motorized actuators. The same tile and CFRP subframe construction will be used for the 2.8 m diameter secondary and (flat) 2.6×3.6 m tertiary. The secondary will be mounted on a hexapod positioner. The tertiary will be mounted on a rotator which will direct the beam to either of the 2 Nasmyth foci.

Optical alignment is a critical issue for CCAT. Tiles will be set on the segments to a few μm rms, based on measurements with a coordinate measuring machine. We do not plan to make subsequent adjustments to the tiles. The segments will be placed to a few $\times 10$ μm rms using laser tracker measurements. The same approach will be used to position the secondary and tertiary mirrors. Initial alignment will be much easier if the primary truss is made of CFRP because thermal deformations will be just a few μm rms during the night. Following initial mechanical alignment, we will switch to astronomical measurements. These will begin with fairly quick through-focus holography[21, 22] to generate look-up tables for low-order gravitational and thermal deformations, or sensor offsets. Final alignment will be based on high-order wavefront measurements using Mars, Uranus and Neptune. These measurements will take tens of minutes to hours, depending on which planets are visible.[23] Alignment maintenance will be based on regular through-focus holography, to check low-order deformations, aperture efficiency measurements, to check the overall wavefront error, and occasional high-order wavefront measurements. Through-focus holography and aperture efficiency measurements can be done with a science camera, but high-order wavefront measurements will require a dedicated instrument, or maybe an interferometer package in front of a science camera. Submillimeter pointing measurements will be made often, probably every $1/2$ hr, using a science camera. CCAT will have at least one small optical telescope for measuring the pointing model (and perhaps also for offset guiding).

Table 3. CCAT half wavefront and pointing errors at $\lambda = 350$ μm.

| Contribution	HWFE	Pointing error	Notes
	μm rms	arcsec rms	
Aberrations	3.65	0	RC design, 5' field angle
Primary, CFRP truss	7.51	0.03	Open-loop control
Primary, steel truss	6.57	0.53	Closed-loop control
Secondary	6.22	0.10	
Tertiary	4.56	0.10	
Instrument	0.05	0.04	
Mount	0	0.13	No HWFE from mount
Alignment	2.19	0.1	Point every 1/2 hr
Telescope total, CFRP truss	11.58	0.22	Quadrature sum of above contributions
Telescope total, steel truss	11.00	0.58	
Goal	10	0.35	<25% increase in integration time, pointing error < beamwidth/10
Atmosphere, 1st quartile	2.5	0.23	At ALMA site, includes daytime
Atmosphere, 2nd quartile	5.0	0.46	
Atmosphere, 3rd quartile	10.9	1.02	
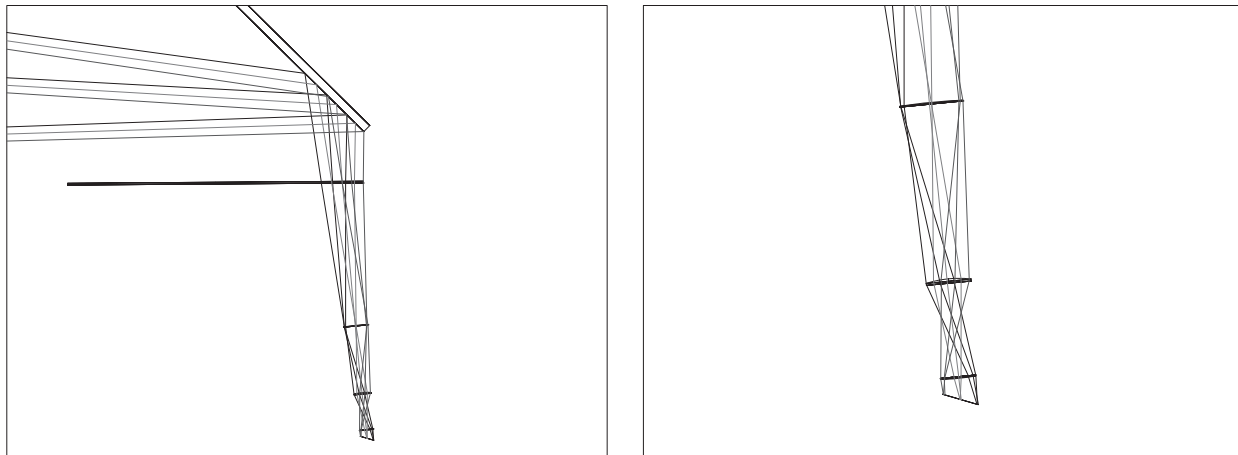
Figure 7. Sub-field camera layout (left) and relay details (right). The tertiary is at the top of the diagram on the left. The corrector plate (2.5 m diameter) is immediately below.

4. WIDE-FIELD CAMERAS

CCAT will be equipped with wide-field cameras covering the 0.2 to 2 mm band. For millimeter wavelengths, we plan to use antenna-coupled pixels. The printed beamforming network in each pixel will contain a filterbank with a few channels, each feeding a microwave kinetic inductance detector (MKID).[24] At submillimeter wavelengths, the plan is to use multichroic splitters feeding separate arrays of absorber-coupled MKIDs. It is difficult to package all the bands in a single instrument, so we are planning 2 separate instruments: a long-wavelength camera and a short-wavelength camera.[25] The first-light MOS will probably be a few Z-spec instruments[26] fed by reconfigurable periscopes.[27]

CCAT's cameras will require some relay optics to transform the $F = 6$ Nasmyth focus to $\mathcal{F} \sim 3$ for the detectors. The submillimeter detectors will have $\sim 0.5 \times 0.5$ mm absorbers,[28] so a $0.5 \mathcal{F} \lambda$ spacing at $\lambda = 350$ μm will require $\mathcal{F} \sim 3$. The millimeter-wave detectors will have $\sim 4 \times 4$ mm antenna arrays,[29] which will require $\mathcal{F} = 2$ to 4 for a detector spacing of $\mathcal{F} \lambda$ to $2\mathcal{F} \lambda$ at $\lambda = 1$ mm. At millimeter wavelengths, the background is small, so the relay must use mirrors or cold lenses. At shorter wavelengths, room temperature lenses are an option. A reflective relay that can be used by all instruments is attractive, but this is not very practical for 1°
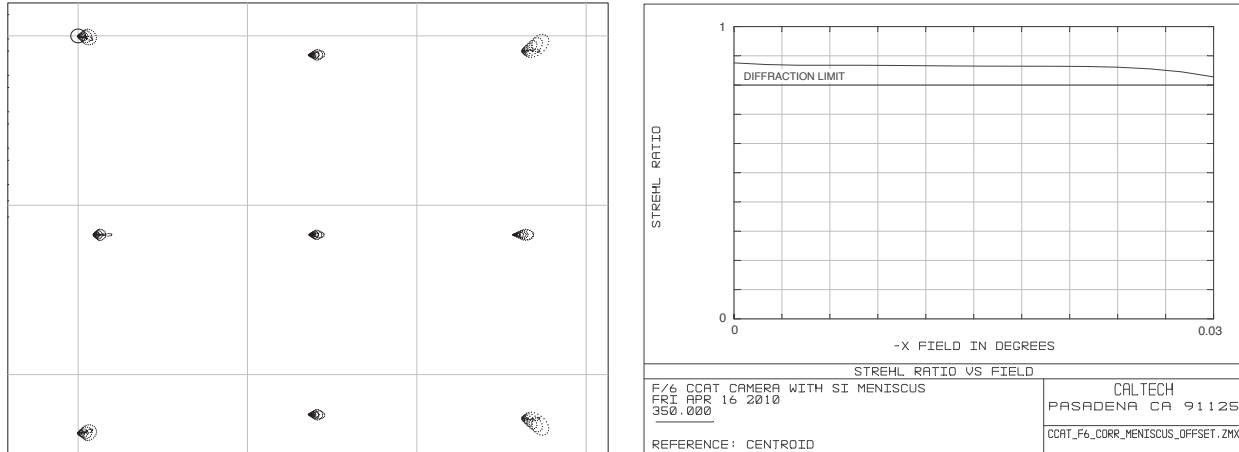
Figure 8. Full-field spot diagram with 1.8' spot spacing (left), and Strehl ratio vs. field angle at $\lambda = 350$ μm (right) for a sub-field camera at 0.4° field angle. The circle in the top left spot diagram is the Airy disc at $\lambda = 350$ μm. The Strehl ratio plot shows the worst case. x is vertical in Fig. 7.

FoV because the mirrors are ~ 10 m in diameter. The only viable approach for such a wide FoV is to break the field up into smaller pieces. The field selection must be done at a focus because that is the only place where beams from adjacent fields do not overlap. It is difficult to close-pack many reflective relays in such a scheme, so a refractive relay seems the best option. The concept for wide field cameras for CCAT uses a field lens at Nasmyth focus to select a sub-field. One or more additional lenses in the camera generate a pupil for a cold stop and an image on the detector. The camera optics fit within a cylinder defined by the field lens, so cameras can be close-packed to efficiently fill the FoV. Fig. 7 shows one possible configuration for the camera optics. The 1st (field) lens in Fig. 7 selects a patch from the Nasmyth focus and transforms it to a pupil for a ~ 1 K cold stop. It is important that the pupil be small to give good control of excess loading, which is a serious concern for absorber-coupled detectors. At the 1st lens, the beam is $(\lambda/200\ \mu\text{m}) \times 1.5$ mm diameter, so small imperfections in the lens will not degrade the image quality. The 2nd (aspheric meniscus) lens refocuses the beam onto the detectors at $\mathcal{F} \sim 3$. The 3rd lens (close to the detectors) makes the final focus roughly telecentric. Fig. 8 shows the image quality for this scheme. A reasonable Strehl ratio can be achieved over 4' FoV at $\lambda = 350$ μm using Si lenses. The maximum diameter of the lenses, filters, and windows in this design is only 175 mm. Components of this size have already been demonstrated in existing millimeter-wave cameras, e.g., MBAC.[12] Since all the lenses are cold, high-density polyethylene is also an option. This would reduce the cost, at the expense of slightly worse image quality. We have proposed to build a prototype sub-field camera, called ATACamera, to test the concept shown in Fig. 7 at the Caltech Submillimeter Observatory. ATACamera will have 128×128 detectors at $\lambda = 350$ μm and 64×64 detectors at $\lambda = 850$ μm. It will serve as the first-light camera for CCAT, or as one sub-field camera in a larger first-light instrument.

A 1° FoV requires ~ 100 5' sub-field cameras. It is obviously impractical to build 100 completely separate cameras, but sub-field cameras can be packed together in, e.g., 7 close-packed cryostats. In this scheme, the camera cryostats will be loaded into a non-rotating instrument tube through the telescope elevation bearing, as shown in Fig. 9. This requires a ~ 3 m diameter clear path along the elevation axis, which is a fairly severe constraint on the mechanical design of the primary truss and elevation bearings. The 2 instrument tubes (one on each side of the telescope) can accommodate 2 wide-field instruments, or many smaller instruments (e.g., one instrument tube might have a short-wavelength camera on the elevation axis, surrounded by a ring of 6 longer-wavelength cameras). Switching between the smaller instruments requires simply a change in pointing. An empty instrument tube can pass a 0.8° FoV through to the Nasmyth platform, so we also have the option of mounting instruments and relay optics on the platform. This approach will probably be used to accommodate large, existing instruments. In Fig. 9, all the connections to the instruments are on the back, so it is possible to quickly install an instrument that is waiting, cold and cabled, on the Nasmyth platform. The sub-field camera approach allows for staged deployment. It is also attractive for a large collaboration like CCAT because the
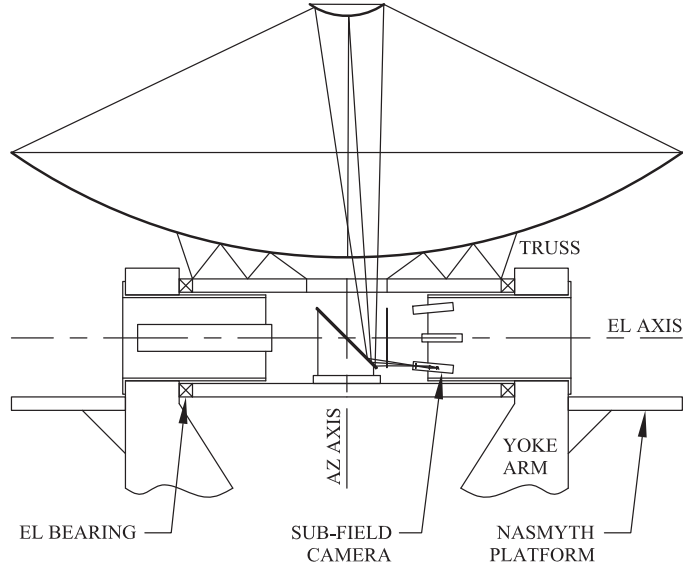
Figure 9. Instrument layout. This is a section through the azimuth and elevation axes with the telescope pointing at zenith. The right Nasmyth focus has a 1° FoV, short-wavelength camera with 5' sub-field cameras. The left Nasmyth focus has a single, 1 m diameter instrument package on the elevation axis. The instruments are attached to the yoke arms, so they do not rotate as the telescope moves in elevation.

partners can share construction of the cameras.

5. EXISTING INSTRUMENTS ON CCAT

Most CCAT survey observations will use new cameras and spectrometers, but some projects may require legacy instruments, e.g., SCUBA-2 and the MUlti-wavelength Submillimeter Inductance Camera (MUSIC). MUSIC has 24×24 pixels, each with $\lambda = 0.85$, 1.0, 1.3, and 2.0 mm detectors.[30,31] The camera is in a downward-looking cryostat, 0.7 m in diameter $\times 2$ m long. MUSIC can be used on CCAT with a relay that has 2 off-axis, ellipsoidal mirrors and 2 flat mirrors, as shown in Fig. 10. This will require a new cold stop and lens, and the cryostat window will have to be extended ~ 0.15 m. In this configuration, MUSIC will have a 7' FoV, with $\sim 1\mathcal{F}\lambda$ pixels at $\lambda = 2$ mm and $\sim 2\mathcal{F}\lambda$ pixels at $\lambda = 850$ μm. The optical design provides a 14' FoV at $\lambda = 750$ μm, which could accommodate an upgraded MUSIC with 48×48 pixels and a 5th observing band at $\lambda = 750$ μm.

SCUBA-2 has 5k detectors at $\lambda = 450$ μm and 5k detectors at $\lambda = 850$ μm in a large cryostat containing a reflective relay.[9] The instrument can be used on CCAT without modification, but it will require an external focal reducer as shown in Fig. 11. On CCAT, the $\lambda = 450$ μm detector array will cover a 2.6' FoV with $0.5\mathcal{F}\lambda$ pixels. The Strehl ratio will be >0.9 over this FoV. The external focal reducer will fit inside one of the CCAT instrument tubes, with the SCUBA-2 cryostat sitting on the Nasmyth platform.

6. SUMMARY

CCAT will emphasize wide-area photometric and spectroscopic surveys with a large telescope optimized for high throughput. It will be equipped with wide-field, multi-color cameras and multi-object spectrometers covering the entire submillimeter band. CCAT will support instruments with up to 1° field of view. We plan to break this field into smaller pieces, each with its own sub-field instrument. This approach will allow us to develop and deploy instruments in stages, taking full advantage of new detector technologies as they become available.
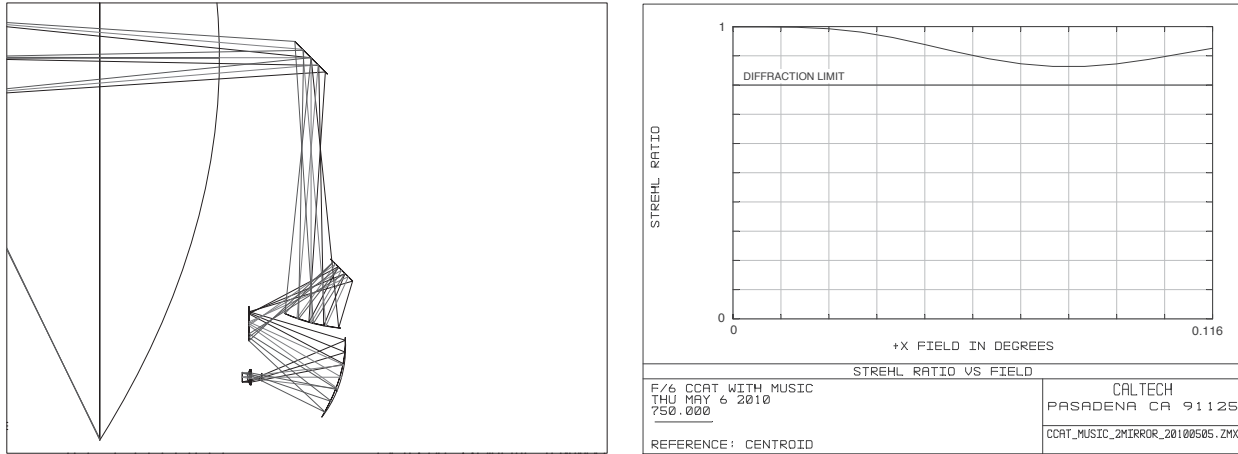
Acknowledgements

Figure 10. Optical layout for MUSIC on CCAT (left) and Strehl ratio vs. field angle at $\lambda = 750\ \mu$m (right). The rays are for field angles of $-7'$, 0, and $+7'$. The tertiary major axis is 1.53 m. The Strehl ratio plot shows the worst case.

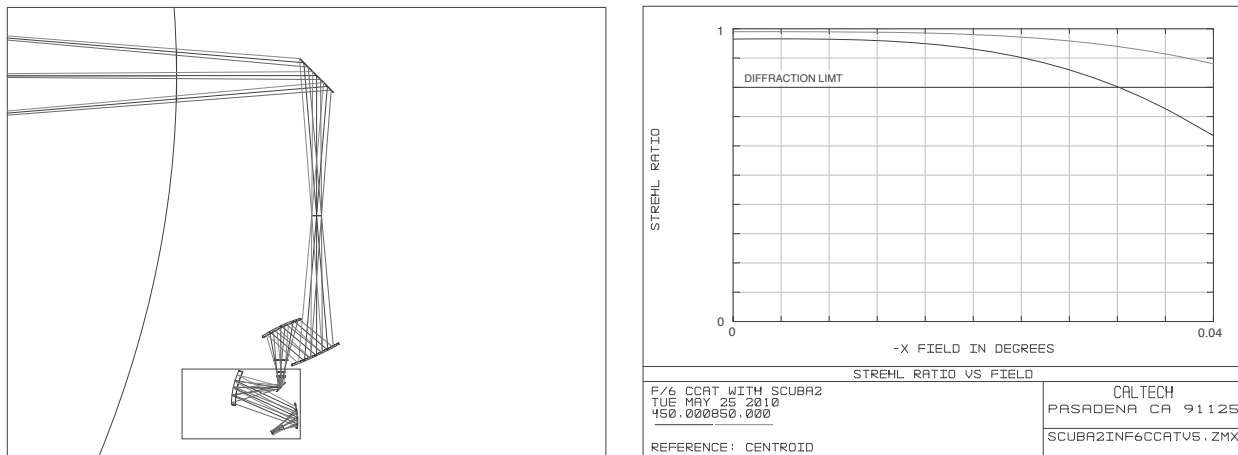Figure 11. Optical layout for SCUBA-2 on CCAT (left) and Strehl ratio vs. field angle (right) at $\lambda = 850\ \mu$m (upper curve) and $\lambda = 450\ \mu$m (lower curve). The layout shows all offsets in the same plane, but offsets after the tertiary would actually be rotated about the elevation axis to give the correct mounting orientation for the cryostat. The rays are for field angles of $-2.4'$, 0, and $+2.4'$. The tertiary major axis is 1.03 m. The Strehl ratio plot shows the worst case.

REFERENCES

1. Radford, S. J. E., Giovanelli, R., Gull, G. E. and Henderson, C. P., "Submillimeter observing conditions on Cerro Chajnantor," Proc. SPIE 7012, 70121Z (2008).

2. Giovanelli, R., Darling, J., Henderson, C., Hoffman, W., Barry, D., Cordes, J., Eikenberry, S., Gull, G., Keller, L., Smith, J. D. and Stacey, G., "The Optical/Infrared Astronomical Quality of High Atacama Sites. II. Infrared Characteristics," PASP 113, 803–813 (2001)

3. Blain, A. W., Smail, I., Ivison, R. J, Kneib, J.-P. and Frayer, D. T., "Submillimeter Galaxies," Phys. Rep. 369, 111–176 (2002).

4. Negrello, M., Perrotta, F., Gonzalez-Nuevo Gonzalez, J., Silva, L., De Zotti, G., Granato, G. L., Baccigalupi, C. and Danese, L., "Astrophysical and cosmological information from large-scale submillimetre surveys of extragalactic sources," Mon. Not. R. Astron. Soc. 377, 1557–1568 (2007).

5. Carlstrom, J. E., Holder, G. P. and Reese, E. D., "Cosmology with the Sunyaev-Zel'dovich Effect," Annu. Rev. Astron. Astrophys. 40, 643–680 (2002).

6. Loewen, N., Brzezik, W., Halliday, D. J. and Sebring, T., "Feasibility study of calotte enclosure for Cornell Caltech Atacama Telescope," Proc. SPIE 6267, 62672J (2006).

7. Loewen, N, Brzezik, W., Fitzsimmons, J., Halliday, D. J., Sun, S. and Vasiljevic, A., "Conceptual design of enclosure for Thirty Meter Telescope," Proc. SPIE 6267, 62672I (2006).

8. Wilson, R. N., "Reflecting Telescope Optics I," Springer-Verlag, Berlin, ch. 2 (1996).

9. Holland, W., et al., "SCUBA-2: a 10,000-pixel submillimeter camera for the James Clark Maxwell Telescope," Proc. SPIE 6275, 62751E (2006).

10. Griffin, M. W., Bock, J. J. and Gear, W. K., "Relative performance of filled and feedhorn-coupled focal-plane architectures," Appl. Opt. 41, 6543–6554 (2002).

11. Lamb, J. W., "Miscellaneous data on materials for millimetre and submillimetre optics," Int. J. Infrared and Millimeter Waves 17, 1997–1132 (1996).

12. Fowler, J. W., Niemack, M. D., Dicker, S. R., Aboobaker, A. M., Ade, P. A. R., Battistelli, E. S., Devlin, M. J., Fisher, R. P., Halpern, M., Hargrave, P. C., Hincks, A. D., Kaul, M., Klein, J., Lau, J. M., Limon, M., Marriage, T. A., Mauskopf, P. D., Page, L., Staggs, S. T., Swetz, D. S., Switzer, E. R., Thornton, R. J. and Tucker, C. E., "Optical design of the Atacama Cosmology Telescope and the Millimeter Bolometric Array Camera," Appl. Opt. 46, 3444–3454 (2007).

13. Tran, H. and Page, L., "Optical Elements for a CMBPol Mission," in Technology Development for a Cosmic Microwave Background Probe of Inflation, eds. S. Hanany and K. Irwin, Journal of Physics Conference Series 155, 012007 (2009).

14. Lau, J., Fowler, J., Marriage, T., Page, L., Leong, J., Wishnow, E., Henry, R., Wollack, E., Halpern, M., Marsden, D. and Marsden G., "Millimeter-wave antireflection coating for cryogenic silicon lenses," Appl. Opt. 45, 3746–3751 (2006).

15. http://www.submm.org/site/weather/

16. Woody, D. P., Padin, S. and Sebring, T., "CFRP truss for the CCAT 25 m diameter submillimeter-wave telescope," Proc. SPIE 7733, 7733-79 (2010).

17. Woody, D. P., Serabyn, E. and Shinkel, A., "Measurement, modeling, and adjustment of the 10.4-m diameter Leighton telescopes," Proc. SPIE 3357, 474–485 (1998).

18. Serabyn, E., Phillips, T. G. and Masson, C. R., "Surface figure measurements of radio telescopes with a shearing interferometer," Appl. Opt. 30, 1227–1241 (1991).

19. Holdaway, M. A., "Calculation of Anomalous Refraction on Chajnantor," MMA Memo 186, NRAO, Charlottesville, VA (1997).

20. Woody, D., MacDonald, D., Bradford, M., Chamberlin, R., Dragovan, M., Goldsmith, P., Lamb, J., Radford, S. and Zmuidzimas, J., "Panel options for large precision radio telescopes," Proc. SPIE 7018, 70180T (2008).

21. Nikolic, B., Hills, R. E. and Richer, J. S., "Measurement of antenna surfaces from in- and out-of-focus beam maps using astronomical sources," Astron. Astrophys. 465, 679–683 (2007).

22. Nikolic, B., Prestage, R. M., Balser, D. S., Chandler, C. J. and Hills, R. E., "Out-of-focus holography at the Green Bank Telescope," Astron. Astrophys. 465, 685–693 (2007).

23. Serabyn, E., "Fundamental limits to wavefront sensing in the submillimeter," Proc. SPIE 6275, 62750Z (2006).

24. Day, P., LeDuc, H. G., Mazin, B. A., Vayonakis, A. and Zmuidzinas, J., "A broadband superconducting detector suitable for use in large arrays," Nature 425, 817–821 (2003).

25. Stacey, G. L. et al., "Instrumentation for the CCAT telescope," Proc. SPIE 6275, 62751G (2006).

26. Inami, H., Bradford, M., Aguirre, J., Earle, L., Naylor. B., Matsuhara, H., Glenn, J., Nguyen, H., Bock, J. J., Zmuidzinas, J and Ohyama, Y., "A broadband millimeter-wave spectrometer Z-spec: sensitivity and ULIRGs," Proc. SPIE 7020, 70201T (2008).

27. Goldsmith, P. F. and Seiffert, M., "A flexible quasioptical input system for a submillimeter multiobject spectrometer," PASP 121, 735–742 (2009).

28. LeDuc, H. G., Bumble, B., Day, P. K., Turner, A., Eom, B. H., Golwala, S., Moore, D., Noroozian, O., Zmuidzinas, J., Gao, J., Mazin, B. A., McHugh, S. and Merrill, A., "Titanium Nitride Films for Ultrasensitive Superconducting Microresonator Detectors," Appl. Phys. Lett., submitted.

29. Schlaerth, J. A., Czakon, N. G., Day, P. K., Downes, T. P., Duan, R. P., Gao, J., Glenn, J., Golwala, S. R., Hollister, M. I., LeDuc, H. G., Maloney, P. R., Mazin, B. A., Noroozian, O., Nguyen, H. T., Sayers, J., Siegel, S., Vaillancourt, J. E., Vayonakis, A., Wilson, P. R. and Zmuidzinas, J., "MKID multicolor array status and results from DemoCam," Proc. SPIE 7741, 7741-8 (2010).

30. Maloney, P. R., Czakon, N. G., Day, P. K., Downes, T. P., Duan, R. P., Gao, J., Glenn, J., Golwala, S. R., Hollister, M. I., LeDuc, H. G., Mazin, B. A., Noroozian, O., Nguyen, H. T., Sayers, J., Schlaerth, J. A., Siegel, S., Vaillancourt, J. E., Vayonakis, A., Wilson, P. R. and Zmuidzinas, J., "MUSIC for sub/millimeter astrophysics," Proc. SPIE. 7741, 7741-15 (2010).

31. Sayers, J., Czakon, N. G., Day, P. K., Downes, T. P., Duan, R. P., Gao, J., Glenn, J., Golwala, S. R., Hollister, M. I., LeDuc, H. G., Maloney, P. R., Mazin, B. A., Noroozian, O., Nguyen, H. T., Schlaerth, J. A., Siegel, S., Vaillancourt, J. E., Vayonakis, A., Wilson, P. R. and Zmuidzinas, J., "Optics for MUSIC: a new (sub)millimeter camera for the Caltech Submillimeter Observatory," Proc. SPIE. 7741, 7741-32 (2010).